Stationary and Oscillatory Localized Patterns, and Subcritical Bifurcations

Vladimir K. Vanag and Irving R. Epstein
Department of Chemistry and Volen Center for Complex Systems, Brandeis University, MS 015, Waltham, Massachusetts 02454-9110, USA
(Received 10 August 2003; published 24 March 2004)

Stationary and oscillatory localized patterns (oscillons) are found in the Belousov-Zhabotinsky reaction dispersed in Aerosol OT water-in-oil microemulsion. The experimental findings are analyzed in terms of subcritical Hopf instability, subcritical Turing instability, and their combination.

DOI: 10.1103/PhysRevLett.92.128301 PACS numbers: 82.40.Ck, 02.70.Uu, 68.05.Gh, 82.33.Nq

Localized patterns, including solitons [1,2], moving, stationary, and breathing spots [3–6], oscillatory peaks [7], localized traveling waves in binary-fluid convection [8], and localized microstructures in solidification [9], are well known in physics. The occurrence of temporally oscillatory, spatially stationary localized patterns (spots), like the oscillons found in a vibrating layer of sand [10], is considerably rarer. Localized oscillatory patterns (clusters) have been found in the Belousov-Zhabotinsky (BZ) reaction-diffusion system subjected to global feedback [11] or periodic perturbation [12]. However, localized oscillons in *autonomous* reaction-diffusion systems have not yet been reported. Here we present observations of oscillons found in the $Ru(bpy)_3^{2+}$- and ferroin-catalyzed BZ reactions dispersed in an Aerosol OT (AOT) microemulsion (BZ-AOT system). We suggest a theoretical explanation for this phenomenon, supported by a numerical solution of a model reaction-diffusion system.

An AOT microemulsion consists of nanometer-sized water droplets dispersed in a continuous oil (octane) phase. Each droplet is surrounded by a surfactant (AOT) monolayer. The polar BZ reagents are dissolved in the aqueous phase, i.e., in the water droplets. Some intermediates, particularly Br_2 and $BrO_2^{\bullet}$, are soluble in the oil phase and can diffuse significantly faster than the water-soluble inhibitor (Br^-) and activator ($HBrO_2$). We refer to Br_2 and $BrO_2^{\bullet}$ as the fast-diffusing inhibitor and fast-diffusing activator, which are chemically linked with Br^- and $HBrO_2$, respectively. These fast-diffusing species are responsible for the rich dynamical behavior of the BZ-AOT system, including Turing structures, packet and standing waves [13,14].

A small droplet (about 0.1 mL) of reactive microemulsion loaded with the components of the BZ reaction is sandwiched between two flat windows separated by an annular Teflon gasket (Zefluor membrane) of thickness 80 μm, inner diameter 25 mm, and outer diameter 47 mm. This arrangement constitutes our reactor. The edges of the reactor are sealed with Teflon tape, and then the two windows are pressed together. Patterns are observed at 23.5 °C through a microscope equipped with a charge-coupled device camera. The reactor is illuminated through 450 or 510 nm interference filters for the $Ru(bpy)_3^{2+}$ or ferroin catalysts, respectively. Our closed batch reactor has the advantage of being homogeneous, while gradients of reactant concentrations are always present in continuously fed unstirred reactors.

In a broad range of initial reagent concentrations and below the percolation threshold (when the volume droplet fraction, φ_d, is less than 0.5), both systems generate Turing patterns [Figs. 1(a) and 1(b)] [13]. For example, in the ferroin-catalyzed system, Turing patterns are found when $[H_2SO_4]_w = [NaBrO_3]_w$ ranges from 0.1 to 0.2 M at $[MA]_w = 0.25$ M. Note that the boundary between the domains of homogeneous steady state and

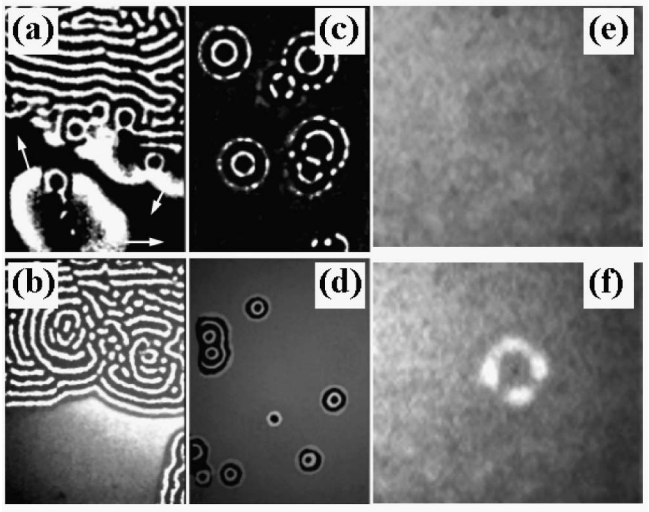

FIG. 1. Turing patterns (a),(b), localized Turing patterns (c), and oscillons (d)–(f) in the $Ru(bpy)_3^{2+}$- (a),(c),(e),(f) and ferroin- (b),(d) catalyzed BZ-AOT systems. Period of the oscillon is 47 s for (e),(f) and about 250 s for (d). $\varphi_d = 0.36$ (a),(d), 0.48 (b), 0.41 (c),(e),(f), $\omega \equiv [H_2O]/[AOT] =$ (a),(c),(e),(d) 15, (b),(d) 18.3, $[H_2SO_4]_w/M =$ (a) 0.32, (c),(e),(f) 0.25, (b),(d) 0.1, $[NaBrO_3]_w/M =$ (a) 0.215, (c),(e),(f) 0.2, (b),(d) 0.1 $[MA]_w = 0.25$ M, $[Ru(bpy)_3^{2+}]_w = [ferroin]_w = 4.2$ mM (subscript w refers to concentrations in the aqueous phase). Frame size, mm^2 = (a)–(c) 5.1×3.75, (d) 7.6×5.6, (e),(f) 2.13×1.87. Arrows in (a) mark directions of phase waves.

Turing patterns depends not only on the BZ reactant concentrations but also on φ_d and the droplet radius. The concentrations in Fig. 1(d) lie on this boundary for $\varphi_d = 0.36$, but for $\varphi_d = 0.48$ [Fig. 1(b)], Turing patterns can be found at even smaller concentrations. A BZ-AOT system of the same composition in a stirred tank reactor exhibits large-amplitude bulk oscillations, which implies that Turing and Hopf modes can interact in a thin unstirred layer, affecting the manner of spreading of the Turing patterns. In the $Ru(bpy)_3^{2+}$-catalyzed system, Turing patterns generate phase waves [Fig. 1(a)] behind which new fragments of Turing patterns emerge. With ferroin, the homogeneous area not occupied by Turing patterns exhibits bulk oscillations [Fig. 1(b)], and each new bulk oscillation adds a new stationary stripe to the Turing pattern.

In both systems, in a narrow range of initial reagent concentrations and φ_d, just below the Hopf bifurcation (a reference stirred system of the same composition shows no bulk oscillations in a tank reactor), localized stationary rings first emerge [Fig. 1(c)] in part of the reactor. We interpret these structures as localized Turing patterns induced by a subcritical Turing instability, like that first found numerically in the Lengyel-Epstein model [15,16]. The necessary finite amplitude localized perturbation may be induced by dust particles in the microemulsion, which serve as the centers of the rings, a hypothesis which also explains the circular shape of the structures.

After about 1 h, these ring patterns (or individual spots or groups of spots) start to oscillate, while their centers remain fixed. Figure 1(d) shows several oscillatory rings for the ferroin-catalyzed system. Two antiphase snapshots of a localized oscillatory ring, remote from the other structures, are shown in Figs. 1(e) and 1(f) for the $Ru(bpy)_3^{2+}$-catalyzed system. Oscillations with a period about 50 s persist for 1–2 h for the $Ru(bpy)_3^{2+}$-catalyzed system, so we can consider these oscillations as quasistationary. For the ferroin-catalyzed system [Fig. 1(d)], we observed only a few oscillations. Small amplitude waves succeed the oscillons, before all patterns eventually disappear in our batch experiment.

Localized oscillatory patterns can be explained on the basis of the phenomenological, but chemically unrealistic, Swift-Hohenberg equation [17–19], or by using reaction-diffusion equations that exhibit a subcritical Hopf bifurcation [20]. Subcritical Hopf bifurcation in a quintic amplitude equation can also give rise to stable localized pulselike solutions [21]. The notion of subcritical Hopf bifurcation as a source of oscillons is an attractive one: for some range of parameters, a system simultaneously possesses a stationary steady state (stationary background) and a stable limit cycle (oscillatory pattern). However, the size and position of the oscillatory region are not determined (even by the size and position of the initial perturbation) and, as simulations show [20], oscillatory regions tend to migrate to the boundary.

Our experiment suggests that *both* subcritical Turing and subcritical Hopf instabilities may be involved in the oscillon phenomenon. Turing instability, characterized by a positive real eigenvalue at some finite wave number $\mathbf{k}_T$ (where the real part has its maximum) possesses an intrinsic wavelength $\Lambda_T = 2\pi/\mathbf{k}_T$, which can restrict the size of the oscillatory region of an oscillon. In the case of subcritical Turing instability, preexisting patterns or superthreshold perturbations can survive even when the eigenvalue of interest is negative.

To examine the possibility of oscillons induced by the interaction of subcritical Turing and Hopf instabilities, we studied two different reaction-diffusion systems that possess subcritical Hopf bifurcations: a model of Ca^{2+} oscillations [22,23], Eqs. (1) and (2) with $k_7 = k_8 = 0$, and a newly developed model of the BZ-AOT system based on the reduced Field-Körös-Noyes model [24] augmented by Br_2 (u) and $BrO_2^\bullet$ (s) in the oil phase [Eqs. (4)–(7)].

$$\partial x/\partial t = k_1 - k_2 x - k_4 x + k_5 y x^4/(K^4 + x^4) + k_6 y - k_7 x + k_8 z + D_x \Delta x, \quad (1)$$

$$\partial y/\partial t = k_4 x - k_5 y x^4/(K^4 + x^4) - k_6 y + D_y \Delta y, \quad (2)$$

$$\partial z/\partial t = k_7 x - k_8 z + D_z \Delta z, \quad (3)$$

where x and y denote the Ca^{2+} concentration in the cytosol and in the endoplasmic reticulum, respectively.

$$\partial x/\partial t = [x(1 - x) + y(q - x) - \beta x + s]/\varepsilon_1 + D_x \Delta x, \quad (4)$$

$$\partial z/\partial t = x - z + D_z \Delta z, \quad (5)$$

$$\partial u/\partial t = [y(q + 2x) - \alpha u/y]/\varepsilon_2 + D_u \Delta u, \quad (6)$$

$$\partial s/\partial t = (\beta x - s)/\varepsilon_3 + D_s \Delta s, \quad (7)$$

where x and z are the normalized concentrations of $HBrO_2$ and oxidized catalyst, respectively, $y = fz/(2q + 3x) + [\alpha u/(2q + 3x)]^{1/2}$ represents $[Br^-]$, and $f = f_0 + u/(K_1 z + u)$.

Though our system is microheterogeneous, the droplet size and the average distance between droplets are 4 orders of magnitude smaller than the Turing wavelength. Therefore, a description of such a system with the aid of "homogeneous" partial differential equations should be valid. We augmented model (1) and (2) by adding a second activator z linearly coupled to the activator x, where z represents the concentration of intercellular Ca^{2+}. This procedure extends the region of subcriticality and gives an important additional eigenvalue for the linearized equations. The second activator serves as a "damping" agent, decreasing (by blurring) the perturbation below a threshold value in the neighborhood of the oscillon.

Systems (1)–(3) and (4)–(7) each have a single steady state, and they have qualitatively similar dispersion curves at appropriate sets of parameters [see Figs. 2(b) and 2(d)]. In the double subcritical region, where both the Hopf and the Turing bifurcations are subcritical and both the real eigenvalue and the real part of the complex eigenvalue are negative, we may expect several types of dynamic behavior: steady states, homogeneous bulk oscillations, Turing patterns, localized (Turing) stationary structures, oscillatory Turing structures (the peaks of the Turing patterns oscillate but do not move), and finally, localized oscillatory structures (oscillons). In numerical simulations with the FLEXPDE package [25], both systems demonstrate all these patterns. Oscillons [Figs. 2(a) and 2(c)] are found only when the real eigenvalue, which is responsible for the Turing instability, has a maximum in the range of wave numbers k where the other pair of eigenvalues, responsible for the Hopf bifurcation, is complex.

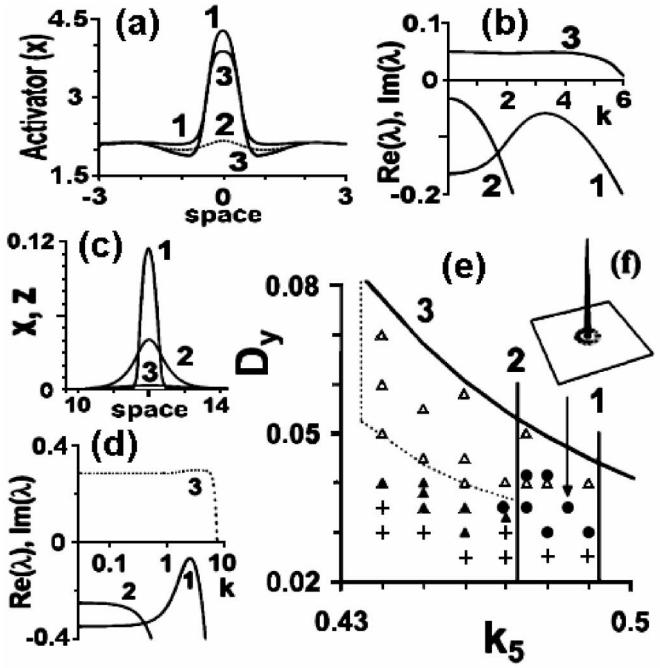

FIG. 2. Oscillon in 1D BZ-AOT model (4)–(7) (c),(d) and oscillon and localized stationary Turing spot in 2D Samogyi-Stucki model (1)–(3) (a),(b),(f). (c) activator (x) (curve 1) and catalyst (z) (curves 2, 3), curve 1 corresponds to curve 2, which is separated in time from curve 3 by $T/2$, $T = 3.46$, (a) cross section of oscillon (curves 1, 2) and stationary spot (curve 3); (f) is a contour map of the oscillon in 2D, area $= 20 \times 20$. (b),(d) Dispersion curves for models (1)–(3) and (4)–(7), respectively: curves 3 and 2 are imaginary part [divided by 6 in (b) and by 10 in (d)] and real part, respectively, of the complex eigenvalue; curve 1 is the real eigenvalue. Parameters for model (1)–(3): $k_1 = 2.1$, $k_2 = 1$, $K = 3.4$, $k_4 = 1.8$, $k_5 = 0.47$, $k_6 = 0.05$, $k_7 = 0.6$, $k_8 = 0.14$, $D_x = D_z = 0.01$, and $D_y = 0.035$. Initial perturbations: $x_0 = x_{SS} + 1.2\cos[0.7\pi(xx^2 + yy^2)^{1/2}]\exp[-0.1(xx^2 + yy^2)]\theta(c^2 - xx^2 - yy^2)$ with center at $xx = yy = 0$, $y_0 = y_{SS}$, $z_0 = z_{SS}$, where xx and yy are spatial coordinates, subscript SS means steady state, and $\theta(a) = 1$ if $a > 0$ and $\theta(a) = 0$ if $a \leq 0$. Oscillon and stationary spot are generated when $c = 2$ and $c = 4$, respectively. Parameters for model (4)–(7): $f_0 = 0.52$ (0.5), $q = 0.0004$, $K_1 = 50$, $\alpha = 0.1$, $\beta = 0.72$, $\varepsilon_1 = 0.05$, $\varepsilon_2 = 0.001$, $\varepsilon_3 = 2$, $D_x = 0.01$, $D_z = 0.3$, $D_u = 1$, and $D_s = 0.028$; (e) $k_5 - D_y$ parameter plane for dynamical behavior of model (1)–(3). Turing patterns occupying the entire area (△), localized Turing patterns (▲), oscillons (●), steady state (+). Vertical lines 1 and 2 mark Hopf and subcritical Hopf bifurcations, respectively; curve 3 is Turing bifurcation.

We have made a more detailed analysis of oscillon behavior in system (1)–(3), which is faster to simulate and may have applications in living systems. An example of an oscillon in 2D is shown in Fig. 2(f) along with its cross section in Fig. 2(a) (curves 1 and 2). At the same parameters, but with a different initial perturbation, a stationary spot [curve 3 in Fig. 2(a)] can be generated instead of the oscillon.

Figure 2(e) shows the variety of behavior obtained in 2D simulations with a localized initial perturbation by varying D_y and k_5. The occurrence of oscillons between curves 1 and 2 is not unexpected, but oscillons are also found to the left of curve 2, where the 0D system (1)–(3) has only a single steady state. In 1D, the region of oscillons and of nonlocal oscillatory Turing patterns is even broader. These patterns are found between the dotted lines and curves 2 and 3 in Fig. 2(e) (oscillatory Turing patterns are also found above curve 3, but we do not consider this region here), which suggests that nonlinear interaction between subcritical Turing and Hopf modes is responsible for the oscillons. For the supercritical case, Turing-Hopf interaction has been studied in coupled amplitude equations [26]. To generate subcriticality, amplitude equations with a destabilizing cubic term need to be augmented with a quintic term [18,27,28]. The relevance of such equations to any reaction-diffusion system is not clear at this point.

In 1D, it is relatively easy to study the sensitivity of an oscillon to initial perturbations. We have chosen a simple toothlike shape of perturbation characterized by amplitude A and width l_p [Fig. 3(a)]. As l_p grows, we find first the homogeneous steady state (SS), then a single stationary peak (1T), then an oscillon (1O), and again the single stationary peak and the steady state. Broad perturbations, with $l_p/\Lambda > 0.4$ (Λ signifies the Turing wavelength, Λ_T), do not give rise to localized structures.

Two local toothlike perturbations separated by a gap g [see upper right of Fig. 3(c)] give us information about the interaction of localized structures. In the $l_p - (g + l_p)$ plane, we see four major areas: SS at small gap, two-peak structures (stationary or oscillatory) at larger g (open symbols), three-peak structures at still larger g (filled symbols), and finally two independent peaks (stationary or oscillatory, depending on l_p) when $g/\Lambda > 2.5$. The

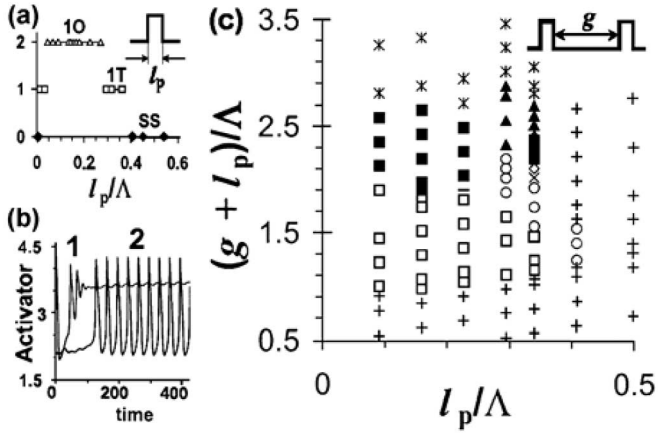

FIG. 3. Dependence of the behavior of model (1)–(3) on initial perturbations in 1D. (a) Toothlike initial perturbation $x_0 = x_{SS} + 1.2\theta[(l_p/2)^2 - xx^2]$ with center at $xx = 0$. Ordinate, which distinguishes among states, is arbitrary. Abbreviations: SS, steady state (assigned ordinate value 0); 1T, single stationary Turing peak (value 1); 1O, single oscillon (value 2); (b) temporal behavior of T + O + T structure ($l_p/\Lambda = 0.34$, $(g + l_p)/\Lambda = 2.7$, $\Lambda = 2.21$), small oscillations in curve 1 (stationary Turing peak) are induced by the oscillatory middle peak. (c) Two identical toothlike initial perturbations separated by a gap of length g. Parameters: $k_1 = 2.1$, $k_2 = 1$, $K = 3.4$, $k_4 = 1.8$, $k_5 = 0.44$, $k_6 = 0.05$, $k_7 = 0.6$, $k_8 = 0.14$, $D_x = D_z = 0.01$, and $D_y = 0.06$. Symbols: +, SS; □, oscillon with two synchronously oscillating peaks; ○, stationary Turing pattern with two peaks; ■, oscillon with three synchronously oscillating peaks; ▲, pattern with three peaks, the middle one oscillating and the outer ones stationary (T + O + T); ×, single oscillon; solid line, single stationary peak; ◇, oscillon with two peaks oscillating antiphase; ∗, two independent Turing or oscillatory peaks.

temporal behavior of one pattern with three peaks is shown in Fig. 3(b). These phenomena suggest that the medium might be employed as a processor for an initial array of pulses (perturbations) with different gaps. Note also that this medium performs *spatial* activation and inhibition by increasing or decreasing the number of initial peaks in the final structure, depending on the gap between peaks. The distance $g = 2.5\Lambda$, above which two peaks behave independently, provides an estimate of the information capacity of the medium as a memory device. An array of N peaks can be in 2^N states, since each peak can be either stationary or oscillatory.

Though we are able to account for our oscillons in terms of interaction between subcritical Turing and subcritical Hopf instabilities, we do not exclude the possibility that subcritical wave instability, in combination, perhaps, with subcritical Turing instability, can provide another explanation for oscillons in this or other systems.

This work was supported by the Chemistry Division of the National Science Foundation.

[1] B. S. Kerner and V.V. Osipov, *Autosolitons: A New Approach to Problems of Self-Organization and Turbulence* (Kluwer, Dordrecht, 1994).
[2] N. J. Zabusky and M. D. Kruskal, Phys. Rev. Lett. **15**, 240 (1965).
[3] E. Ammelt, D. Schweng, and H.-G. Purwins, Phys. Lett. A **179**, 348 (1993).
[4] Yu. A. Astrov and Yu. A. Logvin, Phys. Rev. Lett. **79**, 2983 (1997).
[5] D. Haim *et al.*, Phys. Rev. Lett. **77**, 190 (1996).
[6] K. Krischer and A. Mikhailov, Phys. Rev. Lett. **73**, 3165 (1994).
[7] E. S. Lobanova and F. I. Ataullakhanov, Phys. Rev. Lett. **91**, 138301 (2003).
[8] J. J. Niemela, G. Ahlers, and D. S. Cannell, Phys. Rev. Lett. **64**, 1365 (1990).
[9] H. Jamgotchian, N. Bergeon, D. Benielli, Ph. Voge, B. Billia, and R. Guerin, Phys. Rev. Lett. **87**, 166105 (2001).
[10] P. B. Umbanhowar, F. Melo, and H. L. Swinney, Nature (London) **382**, 793 (1996).
[11] V. K. Vanag, L. Yang, M. Dolnik, A. M. Zhabotinsky, and I. R. Epstein, Nature (London) **406**, 389 (2000).
[12] V. K. Vanag, A. M. Zhabotinsky, and I. R. Epstein, Phys. Rev. Lett. **86**, 552 (2001).
[13] V. K. Vanag and I. R. Epstein, Phys. Rev. Lett. **87**, 228301 (2001).
[14] V. K. Vanag and I. R. Epstein, Phys. Rev. Lett. **88**, 088303 (2002).
[15] O. Jensen, V. O. Pannbacker, G. Dewel, and P. Borckmans, Phys. Lett. A **179**, 91 (1993).
[16] I. Lengyel and I. R. Epstein, Proc. Natl. Acad. Sci. U.S.A. **89**, 3977 (1992).
[17] I. S. Aranson and L. S. Tsimring, Physica (Amsterdam) **249A**, 103 (1998).
[18] H. Sakaguchi and H. R. Brand, Physica (Amsterdam) **117D**, 95 (1998).
[19] M. Tlidi, P. Mandel, and R. Lefever, Phys. Rev. Lett. **73**, 640 (1994).
[20] B. Ermentrout, X. Chen, and Z. Chen, Physica (Amsterdam) **108D**, 147 (1997).
[21] O. Thual and S. Fauve, J. Phys. (Paris) **49**, 1829 (1988).
[22] S. Schuster and M. Marhl, J. Biol. Systems **9**, 291 (2001).
[23] R. Somogyi and J.W. Stucki, J. Biol. Chem. **266**, 11068 (1991).
[24] R. J. Field, E. Körös, and R. M. Noyes, J. Am. Chem. Soc. **94**, 8649 (1972).
[25] FLEXPDE, http://www.pdesolutions.com/flexpde.htm
[26] A. De Wit, D. Lima, G. Dewel, and P. Borckmans, Phys. Rev. E **54**, 261 (1996).
[27] M. C. Cross and P. C. Hohenberg, Rev. Mod. Phys. **65**, 851 (1993).
[28] A. De Wit, Adv. Chem. Phys. **109**, 435 (1999).